White Rose Research Online

eprints@whiterose.ac.uk
https://eprints.whiterose.ac.uk
Universities of Leeds, Sheffield and York

Deposited via The University of Sheffield.

White Rose Research Online URL for this paper:
https://eprints.whiterose.ac.uk/id/eprint/165811/

Version: Accepted Version

Proceedings Paper:
Dolcetti, G. and Krynkin, A. (2018) Development of an optimal array of sensors for the reconstruction of a rigid rough surface based on scattered ultrasound. In: Acoustics 2018. Acoustics 2018 Institute of Acoustics Proceedings, 40 (1). Institute of Acoustics, pp. 164-171. ISBN: 9781906913298. ISSN: 1478-6095.

© 2018 Institute of Acoustics. This is an author-produced version of a paper subsequently published in Institute of Acoustics Proceedings. Uploaded here by permission of the publisher.

Reuse
Items deposited in White Rose Research Online are protected by copyright, with all rights reserved unless indicated otherwise. They may be downloaded and/or printed for private study, or other acts as permitted by national copyright laws. The publisher or other rights holders may allow further reproduction and re-use of the full text version. This is indicated by the licence information on the White Rose Research Online record for the item.

Takedown
If you consider content in White Rose Research Online to be in breach of UK law, please notify us by emailing eprints@whiterose.ac.uk including the URL of the record and the reason for the withdrawal request.

UNIVERSITY OF LEEDS
University of Sheffield
UNIVERSITY of York

DEVELOPMENT OF AN OPTIMAL ARRAY OF SENSORS FOR THE RECONSTRUCTION OF A RIGID ROUGH SURFACE BASED ON SCATTERED ULTRASOUND

G Dolcetti The University of Sheffield, Department of Mechanical Engineering, Sheffield, UK
A Krynkin The University of Sheffield, Department of Mechanical Engineering, Sheffield, UK

1 INTRODUCTION

Traditional ways of measuring the properties of a flow, such as the velocity and depth of rivers, usually require leaving the sensors submerged underwater for long periods of time. This causes larger costs of maintenance and larger potential risks for the operators, which add to the already high cost of the equipment[1]. Alternative techniques based on optics[2], microwave[1], or ultrasound[3], are able to estimate the flow conditions remotely, by measuring the velocity of particles observed right below the water surface, or by measuring the speed of the deformed water-air interface. The behavior of the surface is of large importance also for the exchange of gas, such as CO2, between the flow and the atmosphere[4]. However, the dynamics of this interface are complex and still largely unknown, especially at the small centimetre scale which affect the scattering of light, microwave, and ultrasound, more strongly[3]. As a result, the measurements obtained with these techniques are often unreliable over wide ranges of conditions.

Some of the shortcomings of the remote monitoring techniques mentioned above can be overcome by measuring the shape of the water surface with sufficient resolution, both in time and in space. In this case, in fact, the various types of waves that form on the surface can be identified and isolated[5]. An acoustic technique that allows the spatial measurement of the shape of a rough reflecting acoustically rigid surface (such as the water surface for airborne ultrasound) at subsequent intervals of time, was recently derived[6] and validated experimentally[7]. The method employs approaches that are commonly used in acoustic holography, such as the inversion of an underdetermined system of equations by means of the Singular Value Decomposition[8] (SVD). The linear system is obtained by a linearisation and discretisation of the Kirchhoff integral equation applied to an array of receivers distributed above the surface[6]. In all the previous studies, the shape of the array was chosen arbitrarily. The resulting accuracy was found to be 20% of the surface standard deviation. In this work, the optimal array geometry is identified by means of a genetic optimisation algorithm[9], for a representative parametric surface with zero-gradient in one direction. The sensitivity with respect to the geometrical parameters of the array of the average reconstruction error is studied. The results serve as design guidelines for future implementations of the technique in the field.

This paper is organised as follows: In Section 2 the theoretical background of the method introduced in Ref. 6 is described. Section 3 reports the numerical implementation for this study. The results are shown and discussed in Section 4. Conclusions are drawn in Section 5.

2 THEORETICAL BACKGROUND

2.1 Scattered acoustic field

The surface reconstruction algorithm was previously derived for the case of acoustic propagation in two dimensions[6,7]. Here the method is extended to three-dimensional acoustic waves, although the simple case of a surface with infinite length and constant elevation in the transverse y-direction is considered. In this case, the reconstruction is possible by means of an array of receivers parallel to

the x-z plane following a stationary phase expansion of the Kirchhoff scattering equation along y. All quantities in the derivation reported below are non-dimensionalised with respect to the acoustic wavelength.

A generic surface with zero-gradient in the y-direction is defined explicitly by a function $z = \zeta(x)$ of the sole x–co-ordinate. The x-y plane is defined such that it corresponds to the average of the random surface, $<\zeta>\equiv 0$, where the angular brackets indicate ensemble averaging over multiple realisations of a random process. The y-co-ordinate extends from $-\infty$ to ∞, while the x-co-ordinate extends from $-L/2$ to $L/2$, where L is the surface length. The location of the source is identified by the vector of co-ordinates $\mathbf{S} = (x_s, y_s, z_s)$. Without loss of generality, we consider the case $\mathbf{S} = (0, 0, z_s)$. The scattered acoustic field is measured at a set of locations $\mathbf{R}_m = (x_m, 0, z_m)$, where $m = -M/2, \ldots -1, 1, \ldots M/2$ is an integer index, and M is the number of measurement locations. z_s and z_m are the (positive) distances of the source and receivers from the x-y plane. The reconstruction procedure is based on a Kirchhoff approximation of the scattered field[10], which is valid if $ka_c \sin^3(\varphi) \gg 1$, where $k = 2\pi$ is the non-dimensional acoustic wavenumber, φ is the angle of incidence of the acoustic waves on the surface, measured with respect to the horizontal x-y plane, and a_c is the local radius of curvature, approximated as

$$a_c = \left[1 + \left(\frac{d\zeta}{dx}\right)^{\frac{3}{2}}\right] \left|\frac{d^2\zeta}{dx^2}\right|^{-1}. \tag{1}$$

For the surface implemented for this work, the Kirchhoff parameter was $ka_c > 38$, which is enough to justify the approximation. Then, the acoustic potential field scattered by an acoustically rigid surface is approximated as[10]

$$P(\mathbf{R}_m) = \iint_{\Sigma} \mathbf{n} \cdot \nabla\left[P_I\left(\boldsymbol{\rho}, \mathbf{S}\right) G_0(\mathbf{R}_m, \boldsymbol{\rho})\right] \mathrm{d}\boldsymbol{\rho}, \tag{2}$$

where ∇ represents a spatial gradient, $\mathbf{n}$ is the unit vector normal to the surface, $\boldsymbol{\rho} = \left(x, y, \zeta(x)\right)$ is a vector with the vertex on the surface ζ,

$$G_0(\mathbf{R}_m, \boldsymbol{\rho}) = -\frac{1}{4\pi} \frac{\mathrm{e}^{\mathrm{i}k|\mathbf{R}_m - \boldsymbol{\rho}|}}{\left|\mathbf{R}_m - \boldsymbol{\rho}\right|} \tag{3}$$

is a Green's function, and

$$P_I(\boldsymbol{\rho}, \mathbf{S}) = D(\boldsymbol{\rho}, \mathbf{S}) \frac{\mathrm{e}^{\mathrm{i}k|\boldsymbol{\rho} - \mathbf{S}|}}{\left|\boldsymbol{\rho} - \mathbf{S}\right|} \tag{4}$$

is the incident acoustic field emitted by a source with far-field directivity pattern $D(\boldsymbol{\rho}, \mathbf{S})$.

The source was modelled as a piston with a rigid baffle, with the directivity[11]

$$D(\boldsymbol{\rho}, \mathbf{S}) = 2 \frac{\mathrm{J}_1(ka_s \sin(\vartheta))}{ka_s \sin(\vartheta)}, \tag{5}$$

where J_1 is a Bessel function of the first kind, a_s is the characteristic radius of the piston, and

$$\vartheta(\boldsymbol{\rho}, \mathbf{S}) = \cos^{-1}\left[\frac{z_s - \zeta}{\left|\boldsymbol{\rho} - \mathbf{S}\right|}\right] \tag{6}$$

is the angle between the direction of propagation of the emitted waves and the axis of the source, calculated assuming the source is oriented towards the negative z-axis, i.e., with the largest amplitude of the directivity in the area right below the source.

The following further assumptions have been made:

i) the surface is in the far field with respect to the source and receivers, $k\left|\boldsymbol{\rho}-\mathbf{S}\right| \gg 1$, $k\left|\mathbf{R}_m-\boldsymbol{\rho}\right| \gg 1$;

ii) the surface elevation is small relative to its distance from the source and receiver, $k\zeta^2 / \left|\boldsymbol{\rho}-\mathbf{S}\right| \ll 1$, $k\zeta^2 / \left|\mathbf{R}_m-\boldsymbol{\rho}\right| \ll 1$;

iii) the gradient of the directivity is small, $\nabla D / k \ll 1$;

iv) the surface gradient is small, $\cos(\varphi)d\zeta / dx \ll 1$.

Then,[10]

$$P(\mathbf{R}_m) \approx -\frac{\mathrm{i}}{4\pi}\iint_{\Sigma_0} D(\boldsymbol{\rho}_0,\mathbf{S})\frac{\exp\left\{\mathrm{i}k\left[\left|\boldsymbol{\rho}_0-\mathbf{S}\right|+\left|\mathbf{R}_m-\boldsymbol{\rho}_0\right|\right]-\mathrm{i}q_z(\boldsymbol{\rho}_0,\mathbf{S},\mathbf{R}_m)\zeta(\boldsymbol{\rho}_0)\right\}}{\left|\boldsymbol{\rho}_0-\mathbf{S}\right|\left|\mathbf{R}_m-\boldsymbol{\rho}_0\right|} q_z(\boldsymbol{\rho}_0,\mathbf{S},\mathbf{R}_m)\mathrm{d}\boldsymbol{\rho}_0, \tag{7}$$

where $\boldsymbol{\rho}_0 = (x,y,0)$, and

$$q_z(\boldsymbol{\rho}_0,\mathbf{S},\mathbf{R}_m) = k\left(\frac{z_s}{\left|\boldsymbol{\rho}_0-\mathbf{S}\right|}+\frac{z_m}{\left|\mathbf{R}_m-\boldsymbol{\rho}_0\right|}\right). \tag{8}$$

The integral over the y-co-ordinate can be approximate by a stationary phase expansion with respect to the stationary phase point $y=0$, at each value of x. The result is[12]

$$P(\mathbf{R}_m) \approx \int_{-L/2}^{L/2} H(x,\mathbf{S},\mathbf{R}_m)E(x,\mathbf{S},\mathbf{R}_m)\mathrm{d}x, \tag{9}$$

where

$$H(x,\mathbf{S},\mathbf{R}_m) = -\mathrm{i}\frac{\mathrm{e}^{\mathrm{i}\pi/4}}{4\pi}\sqrt{\frac{2\pi}{k\left[r_m(x,\mathbf{R}_m)+r_s(x,\mathbf{S})\right]}}\frac{D(x,\mathbf{S})q_z(x,\mathbf{R}_m,\mathbf{S})}{\sqrt{r_m(x,\mathbf{R}_m)r_s(x,\mathbf{S})}}\exp\left\{\mathrm{i}k\left[r_m(x,\mathbf{R}_m)+r_s(x,\mathbf{S})\right]\right\}, \tag{10}$$

$$E(x,\mathbf{S},\mathbf{R}_m) = \exp\left[-\mathrm{i}q_z(x,\mathbf{S},\mathbf{R}_m)\zeta(x)\right], \tag{11}$$

$$r_s = \sqrt{x^2+z_s^2}, \tag{12}$$

and

$$r_m = \sqrt{(x-x_m)^2+z_m^2}. \tag{13}$$

2.2 Discretisation and linearisation

The aim of the reconstruction technique is to determine the value of the surface elevation at an equidistant set of N locations $x_i = i\Delta x$, where $i = 0,\pm1,\ldots,\pm(N-1)/2$ is an integer index. In order to do so with the technique proposed in Ref. 6, it is necessary to expand $E(x,\mathbf{S},\mathbf{R}_m)$ with respect to a value which is independent of $\mathbf{R}_m$. For this work, it is suggested to define

$$E(x,\mathbf{S},\mathbf{R}_m) \approx \tilde{E}(x,\mathbf{S}) = \exp\left[-\mathrm{i}\tilde{\mathrm{q}}_z(x,\mathbf{S})\zeta(x)\right], \tag{14}$$

where

$$\tilde{q}_z(x,\mathbf{S}) = 2k\frac{z_s}{r_s(x,\mathbf{S})}. \tag{15}$$

Introducing the approximate Eq. (14) into Eq. (9), and approximating the integral with a discrete sum with respect to x_i, the acoustic field at the location $\mathbf{R}_m$ is

$$P(\mathbf{R}_m) \approx \Delta x \sum_{i=-N/2}^{N/2} H(x_i,\mathbf{S},\mathbf{R}_m)\tilde{E}(x_i,\mathbf{S}), \tag{16}$$

which has the convenient matrix representation

$$\mathrm{P}_{M\times 1} = \mathrm{H}_{M\times N}\tilde{\mathrm{E}}_{N\times 1}, \tag{17}$$

where $\mathrm{P}_{M\times 1}$ is a vector with elements $\mathrm{P}_m = P(\mathbf{R}_m)$ that represents the instantaneous acoustic field measured at each location $\mathbf{R}_m$, $\tilde{\mathrm{E}}_{N\times 1}$ is a vector with elements $\tilde{\mathrm{E}}_i = \tilde{E}(x_i,\mathbf{S})$ which contains the dependence on the surface elevation at the locations x_i, and $\mathrm{H}_{M\times N}$ is a transfer matrix with elements $H_{m,i} = \Delta x H(x_i,\mathbf{S},\mathbf{R}_m)$.

2.3 Inversion

In order for Eq. (16) to approximate Eq. (9) with sufficient accuracy, the spatial grid x_i should sample the x-co-ordinate with good resolution and over a large enough length. As a result, in most practical cases the number of reconstruction locations x_i is larger than the number of measurement locations, $N > M$, and the linear system of Eq. (17) is underdetermined. The authors of Ref. 6 proposed to calculate the vector $\tilde{\mathrm{E}}_{N\times 1}$ by approximating the inverse of the transfer matrix $\mathrm{H}_{M\times N}$ by means of a Singular Value Decomposition (SVD). The larger errors that potentially derived from this approximation can then be reduced by means of a Tikhonov regularization technique, where the regularisation parameter is determined following a Generalised Cross-Validation approach. Details of these calculations are reported in Ref. 6. The final result of this procedure is the approximation of vector $\tilde{\mathrm{E}}_{N\times 1}$ in the form

$$\tilde{\mathrm{E}}_{N\times 1} \approx \mathrm{V}_{N\times M}\mathrm{K}^{-1}_{\beta,M\times M}\mathrm{U}^{T}_{M\times M}P_{M\times 1}, \tag{18}$$

where $\mathrm{V}_{N\times M}$ is a truncated unitary matrix, $\mathrm{U}^{T}_{M\times M}$ is the Hermitian transpose of another unitary matrix, and $\mathrm{K}^{-1}_{\beta,M\times M}$ is the regularised inverse of the matrix of principal values $\mathrm{K}_{M\times M}$, where β is the regularisation parameter.

From the solution of Eq. (18), an estimate of the value of the surface elevation $\zeta(x_i)$ can be calculated by means of Eq. (14) as

$$\tilde{\zeta}(x_i) = -\frac{\Im\left\{\log\left[\tilde{E}(x_i,\mathbf{S})\right]\right\}}{\tilde{q}_z(x_i,\mathbf{S})}, \tag{19}$$

where $\Im$ represents the imaginary part. The accuracy of the reconstruction at each location x_i is represented by the squared error,

$$\varepsilon^2(x_i) = \left[\zeta(x_i) - \tilde{\zeta}(x_i)\right]^2, \tag{20}$$

while the root mean squared error averaged over a portion of the surface with length $L_\varepsilon = N_\varepsilon \Delta x$, $N_\varepsilon \leq N$, is

$$\varepsilon_{\mathrm{rms}} = \sqrt{\frac{1}{N_\varepsilon}\sum_{i=-N_\varepsilon/2}^{N_\varepsilon/2}\varepsilon(x_i)}. \tag{21}$$

3 NUMERICAL IMPLEMENTATION

3.1 Scattering surface model

The reconstruction procedure outlined in the previous section is valid for any rigid surface that satisfies the conditions listed in section 2.1. In this work, we are interested in types of random surfaces that are representative of the shape of the water surface of shallow water flows, such as small rivers. In Ref. 3 and Ref. 13 it has been demonstrated that a reasonably accurate

representation of such surface is provided by a linear random-phase surface model assuming a power-function decay of the spatial Fourier spectrum as a function of the inverse of the surface wavelength, Λ. For a surface with zero-gradient along the y-direction, a single realisation is then obtained as[13]

$$\zeta(x) = \sigma \sqrt{\frac{l_0}{L}\left[\left(\frac{l_0}{l_1}\right)^{1-\alpha} - 1\right]^{-1} 2(\alpha-1)} \sum_{p=L/l_0}^{L/l_1} \eta_p \left(\frac{p l_0}{L}\right)^{-\frac{\alpha}{2}} \cos\left[2\pi p \frac{x}{L} + \phi_p\right], \tag{22}$$

where η_p is a random variable with a normal distribution, ϕ_p is a random variable with uniform distribution between $-\pi$ and π, $\sigma^2 = \left\langle \zeta^2 \right\rangle$ is the variance of the surface elevation, α is the slope of the surface power spectrum, l_0 is the largest wavelength of the surface, l_1 is the smallest wavelength of the surface, and p is an integer index.

According to the model represented by Eq. (22), the surface statistics are identified uniquely by the values of the parameters σ, α, l_0, and l_1. For this work, we considered a surface with $\alpha = 3$ and with the non-dimensional parameters $\sigma = 0.05$, $l_0 = 15$, and $l_1 = 3$. These values are believed to be representative of the free surface of a relatively slow, deep flow[5].

3.2 Array configuration

In Ref. 6 and Ref. 7, the shape of a scattering surface was reconstructed by measuring the scattered acoustic field with arrays of 20 to 121 microphones arranged on a semi-circle with radius of 0.4 m (50.6 in non-dimensional co-ordinates), with an accuracy of 20%. For practical applications, it is more convenient to arrange the microphones along a line with constant distance from the average surface. In this study, it was then preferred to construct the array such that $z_m = z_0 = \text{const.}$, and $x_m = m\gamma_0$, $m = \pm 1, \ldots \pm (M/2)$, where γ_0 is the spacing between the microphones, non-dimensionalised with respect to the acoustic wavelength. For simplicity, it was also assumed that the surface is located at the same height as the microphones, i.e., $z_s = z_0$. A schematic representation of the array is shown in Figure 1.

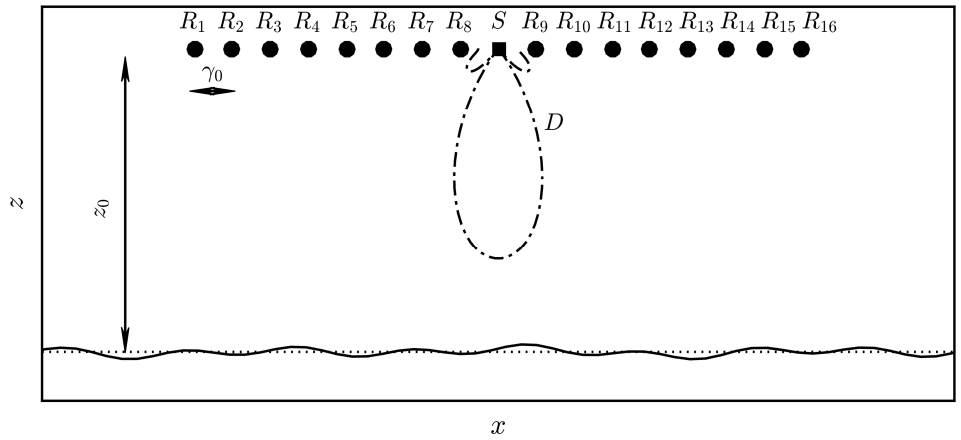

Figure 1: A schematic representation of the measurement setup, with the location of the source, $\mathbf{S}$, location of the microphones, $\mathbf{R}_m$, directivity pattern D, and geometrical parameters of the array, z_0, and γ_0. Dimensions are not to scale.

3.3 Error calculation and optimisation

In order to test the accuracy of the reconstruction numerically, for different choices of the parameters z_0 and γ_0 that define the geometry of the array, 500 realisations of the rough surface identified by different values of the variables η_p and ϕ_p were generated. For each realisation, the values of the complex acoustic field at the M locations $\mathbf{R}_m$ were calculated based on a stationary phase expansion of Eq. (2), analogous to Eq. (7) but without the four approximations listed in Section 2.1. For these calculations, the integral over x was calculated with the quadrature method after discretisation, using a finer grid than the one employed for the reconstruction, with a non-dimensional spacing of 0.01 and extending between -30 and 30 in units of the acoustic wavelength. The characteristic radius of the source was chosen as $a_s = 2.5$. This produced a directivity pattern characterised by a central lobe with the angular width of approximately 28°.

The reconstruction was performed at $N = 151$ locations x_i, with $\Delta x = 0.2$, and $L = 30$. The number of points where the acoustic field was measured was much smaller in comparison, $M = 16$. The surface reconstruction obtained with the method employed here is known to yield a large overestimation of the surface elevation away from the centre of the insonificated area, where $x_i \sim L/2$. This larger error was found to skew the error distribution considerably. To overcome this limitation, the root mean squared error was averaged only on the central portion of the x-axis, by setting $N_\varepsilon = 0.4N$ in Eq. (21). As a result, the number of useful locations where the surface reconstruction was of sufficient accuracy was limited to $N_\varepsilon = 60$, still larger than M. The accuracy of the reconstruction for the 500 realisations was quantified by the average error

$$\bar{\varepsilon} = \sqrt{\left\langle \varepsilon_{\mathrm{rms}}^2 \right\rangle}. \tag{23}$$

The optimal geometry of the measurement array, identified by the values of z_0 and γ_0, was determined by means of a Self Adaptive Differential Evolution (SADE) algorithm[9], using $\bar{\varepsilon}^2$ as the cost function to minimise. The algorithm is based on the random initialisation and evolution of a number (20 for this study) of populations of the parameters z_0 and γ_0 chosen randomly. At each step of the iteration, every set is modified according to a mutation strategy, which is chosen randomly based on its probability of success during the previous iterations. In this way, the algorithm is able to identify the optimum in the most efficient way, eventually modifying its strategy at different stages of the optimisation.

For this work, the two parameters z_0 and γ_0 were initialised uniformly within the intervals $z_0 \in [10, 100]$ and $\gamma_0 \in [0.2, 20]$. The convergence was monitored in terms of the minimum of $\bar{\varepsilon}$ across each set of parameters, and of its average across all sets. After 139 iterations, the two convergence indicators coincided to within machine precision, indicating that all populations had converged to the same optimum. The optimum was reached by the fastest populations after 104 iterations.

4 RESULTS

For the set of surface parameters and for the value of the characteristic source radius used for this work, the optimal configuration of the array of microphones has been determined in terms of the optimal parameter values $z_0 = 36.6$ and $\gamma_0 = 2.37$. These parameters were found to yield a minimum non-dimensional root mean squared averaged error $\bar{\varepsilon} = 0.007$, which corresponded to 13.5% of the surface standard deviation σ. An example of surface reconstruction obtained with the optimal parameters is shown in Figure 2a.

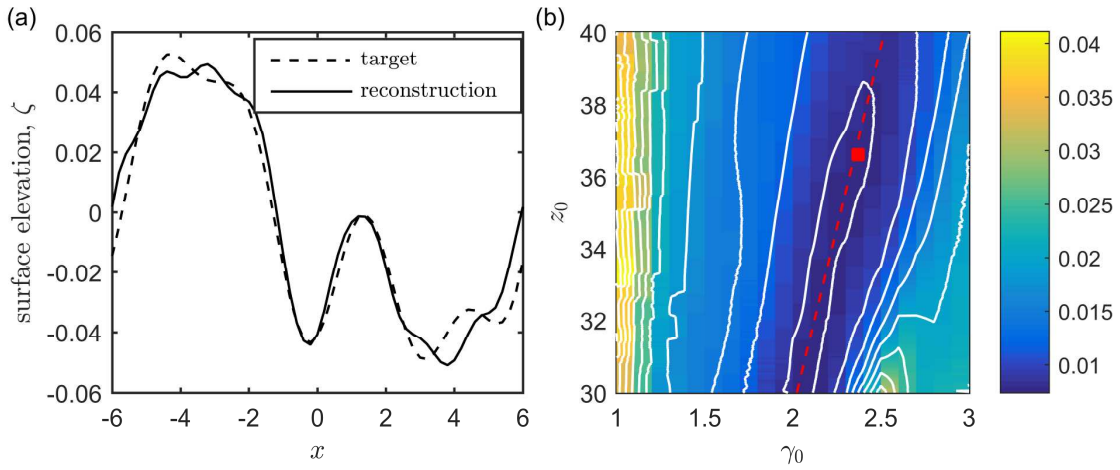

Figure 2: (a) An example of surface reconstruction obtained with an optimised array of 16 microphones. Reconstruction obtained at 151 locations along x. Only the portion of the surface used for the computation of the root mean square averaged error is shown. (dashed) Target surface; (solid) reconstructed surface. (b) Variation of the average reconstruction error with the geometrical parameters z_0, and γ_0. White contours indicate error levels with a variation of 0.003. The red rectangle indicates the optimal combination of γ_0 and z_0 calculated by means of the genetic algorithm. The red dashed line shows the linear relation of Eq. (24).

The convergence parameters were found varying greatly during the optimisation procedure, which indicates a strong influence of the geometry of the array on the accuracy of the reconstruction. In order to better investigate the sensitivity of the error with respect to the parameters z_0 and γ_0, the root mean squared averaged error was calculated explicitly for a range of values of z_0 and γ_0 in the vicinity of the optimal values. These results are shown in Fig. 2b. It can be seen that the error varies greatly for different array geometries, reaching a maximum of $\overline{\varepsilon} = 0.04$, which corresponds to 82% of the surface standard deviation. Therefore, choosing the array geometry arbitrarily without an instrument to predict the accuracy of the reconstruction could lead to very large errors.

Larger errors are found for $\gamma_0 \approx 1$, independently of the value of z_0, and for $\gamma_0 \approx 2.5$, when $z_0 \leq 31$. The optimal configuration belongs to a plateau in the error distribution, characterised by slow variations of the accuracy. Within this region, variations of γ_0 of the order of ± 0.25 have a relatively little effect on the accuracy, increasing the root mean squared average error to less than $\overline{\varepsilon} = 0.011$, or 22% of σ. z_0 potentially has an even smaller effect. In fact, the minimum of the root mean square error calculated for each value of z_0 remains below a maximum value of $\overline{\varepsilon} = 0.008$. In order to maintain the error small, though, every increase of z_0 must be accompanied by a simultaneous increase of γ_0. This means that the microphones need to be more largely spaced as they are moved further away from the surface. The locations of the minimum errors calculated for each value of z_0 were interpolated, resulting in an approximate optimal linear relation between z_0 and γ_0, quantified as

$$z_0 \approx 20.1\gamma_0 - 10.7. \tag{24}$$

5 CONCLUSIONS

The study has demonstrated the possibility to improve the accuracy of the surface reconstruction technique presented in Ref. 6 by almost an order of magnitude, if the optimal location of the acoustic source and array of receivers is selected. The sensitivity of the reconstruction error with respect to the geometry parameters has been investigated. The optimal spacing between the microphones increases almost linearly with an increase of the distance between the array and the surface. If this relation is respected, the error increases only very slightly away from the optimal configuration. Future studies will investigate the effects on the accuracy of the various parameters that determine the surface statistics.

6 ACKNOWLEDGEMENTS

This work was supported by EPSRC Grant No. EP/N029437/1.

7 REFERENCES

1. W.J. Plant, W.C. Keller, and K. Hayes, Measurement of river surface currents with coherent microwave systems, IEEE T. Geosci. Remote 43(6), 1242-1257 (2005).
2. M. Muste, I. Fujita, and A. Hauet, Large-scale particle image velocimetry for measurements in riverine environments, Water Resour. Res. 44(4), W00D19 (2008).
3. G. Dolcetti, A. Krynkin, and K.V. Horoshenkov, Doppler spectra of airborne sound backscattered by the free surface of a shallow turbulent water flow, J. Acoust. Soc. Am. 142(6), 3387-3401 (2017).
4. D.E. Turney and S. Banerjee, Air–water gas transfer and near-surface motions. J. Fluid Mech. 733, 588-624 (2013).
5. G. Dolcetti, K.V. Horoshenkov, A. Krynkin, and S.J. Tait, Frequency-wavenumber spectrum of the free surface of shallow turbulent flows over a rough boundary, Phys. Fluids 28(10), 105105 (2016).
6. A. Krynkin, K.V. Horoshenkov, and T. Van Renterghem, An airborne acoustic method to reconstruct a dynamically rough flow surface. J. Acoust. Soc. Am. 140(3), 2064-2073 (2016).
7. A. Krynkin, G. Dolcetti, and S. Hunting, Acoustic imaging in application to reconstruction of rough rigid surface with airborne ultrasound waves. Rev. Sci. Instrum. 88(2), 024901 (2017).
8. W.H. Press, S.A. Teukolsky, W.T. Vetterling, and B.P. Flannery, Numerical Recipes: The Art of Scientific Computing, 3rd ed., Cambridge University Press, 65–75 (2007).
9. A.K. Qin and P.N. Suganthan, Self-adaptive differential evolution algorithm for numerical optimization. Proc. 2005 IEEE C. Evol. Computat, Vol. 2, 1785-1791 (2005).
10. F.G. Bass and I.M. Fuks, Wave scattering from statistically rough surfaces, Vol. 93 of International Series in Natural Philosophy, Oxford Pergamon Press, 225 (1979).
11. P.M. Morse and K.U. Ingard, Theoretical Acoustics, Princeton University Press, 381 (1968).
12. G.B. Deane, J.C. Preisig, C.T. Tindle, A. Lavery, and M. Dale Stokes, Deterministic forward scatter from surface gravity waves. J. Acoust. Soc. Am. 132(6), 3673-3686 (2012).
13. G. Dolcetti and A. Krynkin, Doppler spectra of airborne ultrasound forward scattered by the rough surface of open channel turbulent water flows. J. Acoust. Soc. Am. 142(5), 3122-3134 (2017).